Front. Struct. Civ. Eng. 2023, 17(5): 722–731
https://doi.org/10.1007/s11709-023-0950-5

RESEARCH ARTICLE

Appraising the potential of calcium sulfoaluminate cement-based grouts in simulated permafrost environments

Jian ZHAO[a], Guangping HUANG[a], Lin LIAO[b*], Wei Victor LIU[a*]

[a] *Department of Civil and Environmental Engineering, University of Alberta, Edmonton T6G 1H9, Canada*
[b] *College of Mining Engineering, Taiyuan University of Technology, Taiyuan 030024, China*
[*]*Corresponding authors. E-mails: liaolin@tyut.edu.cn; victor.liu@ualberta.ca*

ABSTRACT The aim of this study is to appraise the potential of calcium sulfoaluminate (CSA) cement-based grouts in simulated permafrost environments. The hydration and performance of CSA cement-based grouts cured in cold environments (10, 0, and −10 °C) are investigated using a combination of tests, including temperature recording, X-ray diffraction (XRD) tests, thermogravimetric analysis (TGA), and unconfined compressive strength (UCS) tests. The recorded temperature shows a rapid increase in temperature at the early stage in all the samples. Meanwhile, results of the TGA and XRD tests show the generation of a significant quantity of hydration products, which indicates the rapid hydration of CSA cement-based grouts at the early stage at low temperatures. Consequently, the CSA cement-based grouts exhibit remarkably high early strength. The UCS values of the samples cured for 2 h at −10, 0, and 10 °C are 6.5, 12.0, and 12.3 MPa, respectively. The UCS of the grouts cured at −10, 0, and 10 °C increases continuously with age and ultimately reached 14.9, 19.0, and 30.6 MPa at 28 d, respectively. The findings show that the strength of grouts fabricated using CSA cement can develop rapidly in cold environments, thus rendering them promising for permafrost applications.

KEYWORDS permafrost, low temperatures, calcium sulfoaluminate cement-based grouts, hydration reaction, compressive strength

1 Introduction

Grouting is an enhancement technique involving the injection of flowable mixtures (known as grouts) into the fractures or voids of rock or soil mass to stabilize the ground in mining and civil engineering [1–3]. Among the different types of grouts, cement-based grouts are the most frequently used. In particular, ordinary Portland cement (OPC) is widely utilized owing to its advantages of excellent stability, high strength, and low price [4–8]. The performance of OPC-based materials depends primarily on their operating temperatures [9,10]. In permafrost regions, the average annual air temperature is typically below −1 °C [11], the minimum temperatures of soil and rock in underground stopes can reach −10 °C [12,13]. In heated underground stopes, the temperature can be as low as 5 °C [14]. Under such conditions, the strength development of OPC-based materials is hindered significantly. According to Huang et al. [15], the 1-d strength of OPC mortar at 5 °C was only 0.2 MPa. Such slow strength development at low temperatures may cause grouting failure, affect construction efficiency, or significantly threaten the safety of workers.

Compared with OPC, calcium sulfoaluminate (CSA) cement exhibits rapid setting and strength development, rendering it promising for permafrost applications [10,16–18]. CSA cement is a sustainable cement material manufactured via the calcination of bauxite, limestone, and gypsum [19,20]. Unlike OPC, it can reduce the CO_2 footprint by ~35% at the maximum owing to the lower

Article history: Received Aug 30, 2022; Accepted Dec 3, 2022

calcination temperature of the CSA cement clinker (~1250 °C, in contrast to ~1450 °C of OPC) [21]. The CSA cement clinker is primarily composed of ye'elimite ($C_4A_3\overline{S}$) and belite ($\beta-C_2S$) [22,23]. Moreover, other minor phases, including calcium sulfates ($C\overline{S}$), brownmillerite (C_4AF), calcium aluminates (CA, or $C_{12}A_7$), gehlenite (C_2AS), and calcium sulphosilicate ($C_5S_2\overline{S}$) are discovered in CSA cement [24]. CSA cement can hydrate quickly and generate various hydration products, including ettringite ($C_6A\overline{S}_3H_{32}$ or AFt), monosulfoaluminate ($C_4A\overline{S}H_{12}$ or AFm), and aluminum hydroxide (AH_3) [20,24–26].

Owing to the rapid hydration of CSA cement, grouts prepared using CSA cement have the potential to be used in permafrost regions. Currently, only a few studies have been done on CSA cement-based grouts. For instance, Zhang et al. [27] prepared ultrafine CSA cement-based double liquid grouts using various proportions of anhydrite and quicklime. The results showed that the UCS of grouts was the highest when the anhydrite–quicklime ratio was 4:1. Based on this ratio, Zuo et al. [5] investigated the effect of water–binder ratio on the performance of CSA cement-based grouts. Based on their findings, a water–binder ratio of 8:1 could be regarded as a turning point. Beyond this ratio, the hydration heat release in the grouts decreased obviously and the formation of ettringite decelerated. Additionally, the effects of various accelerators (e.g., lithium carbonate, aluminum sulfate, and LiAl-layered double hydroxides) on the performance of CSA cement-based grouts have been investigated [28–30]. These studies demonstrated that incorporating a low amount of accelerator accelerated hydration reactions at the early age and promoted the early compressive strength. Although a few studies have conducted on CSA cement-based grouts, the potential of using CSA cement-based grouts in permafrost environments (e.g., −10 °C) has not been investigated hitherto. There is a need to appraise the potential of CSA cement-based grouts in permafrost environments, ultimately to provide a brand-new solution to fulfill the requirements of rapid strength growth when grouting in permafrost regions.

To this end, this study is performed to appraise the potential of using CSA cement-based grouts cured in simulated permafrost environments. Temperature recording, thermogravimetric (TGA) analysis, and X-ray diffraction (XRD) tests are performed to understand the hydration of CSA cement-based grouts cured at low temperatures. Unconfined compressive strength (UCS) tests are performed to evaluate the strength development of the grouts. This study can provide a valuable theoretical basis for the future applications of CSA cement-based grouts in permafrost environments.

2 Materials and methods

2.1 Materials

The CSA cement-based grouts used in this study are composed of two components: Compositions A and B. Composition A is composed of a CSA cement clinker, Composition B is composed of anhydrite and quicklime mixed in proportions of 4:1 by mass. Researchers have shown that such grouts can achieve the highest compressive strength when anhydrite and quicklime are combined at a ratio of 4:1 by weight [27]. The primary chemical and mineral compositions of the CSA cement clinker are presented in Tables 1 and 2, respectively.

2.2 Sample preparation

Compositions A and B of the CSA cement-based grouts were blended at a ratio of 1:1 such that they can be mixed more easily, thus rendering grouting operations more efficient. A water-to-solid ratio of 0.6 was used to ensure that the grouts satisfied the mechanical performance and workability of grouts simultaneously. Before blending the grouts, Compositions A and B as well as water were stored at 20 °C, and the temperature was controlled at 20 °C to maintain consistency.

Samples of the CSA cement-based grouts were prepared as follows: First, water was added to Compositions A (CSA clinker) and B (anhydrite and quicklime), separately; subsequently, the mixtures were stirred via whisking for 90 s at a speed of 150 $r\cdot min^{-1}$ to form Slurries A and B. The two slurries were mixed

Table 1 Chemical composition of CSA cement clinker

chemical composition	mass (%)
SiO_2	10.59
CaO	45.02
Al_2O_3	29.54
Fe_2O_3	2.21
MgO	1.97
TiO_2	1.45
SO_3	8.45
loss	0.77

Table 2 Main mineral composition of CSA cement clinker

mineral composition	mass (%)
$C_4A_3\overline{S}$	56.44
$\beta-C_2S$	31.19
C_4AF	5.47

rapidly and stirred for 90 s at 150 r·min^{-1}. Finally, the pastes were placed in molds with a diameter of 50 mm and a height of 100 mm. To ensure the compactness of the specimens, the pastes were cast in two layers for each specimen, and each layer was manually tamped 30 times using a tamping rod after casting. All samples were protected with plastic films to prevent water evaporation.

In this study, the samples were cured in cold sand to achieve simulated permafrost environments, as proposed in our previous study [15]. This was performed because frozen sand has a thermal conductivity (1.2–3.6 W·m^{-1}·K^{-1}) similar to that of ground in permafrost regions (1.49–2.24 W·m^{-1}·K^{-1}) [31,32]. As shown in Fig. 1, water-saturated sand was placed in a plastic bucket and a cylindrical steel ring was inserted into it to promptly embed the samples. Subsequently, the bucket was placed in a freezer to cool the sand to a specific temperature. After the pastes were cast in molds, the samples were embedded into rings to begin curing. The sand temperatures in this study were controlled at 10, 0, and −10 °C. Moreover, samples cured at 20 °C in a laboratory environment were used as the reference.

2.3 Methods

2.3.1 Temperature recording

The temperature profile as a function of time allows one to understand the hydration of grouts, which is associated significantly with the strength development and hydration reaction of cement [4]. To investigate the hydration process of grouts at each temperature, the temperature variations exhibited by hardening CSA cement-based grouts were recorded. After casting the samples, temperature sensors were embedded in the centers of the samples to measure the hardening temperatures of the grouts at each curing temperature. Subsequently, a temperature sensor was inserted in sand to record its temperature and verify the curing conditions. All the sensors were connected to a data logger to record the temperature profiles. In this study, Pt100 temperature sensors and an MIK-R200T recorder were used to record the temperatures. The temperature data were recorded every 30 s.

2.3.2 XRD test

XRD tests can be performed to investigate the types and amounts of hydration products in grouts [19]. In this study, these tests were performed to analyze the hydration process of grouts at different temperatures for 2 h and 28 d. Before the XRD tests were performed, small pieces extracted from each sample were immersed in ethyl alcohol for 36 h to halt hydration via solvent exchange and then dried in an oven at 40 °C for 48 h. After desiccation, the pieces were ground and sieved to obtain pieces measuring 150 μm or less.

XRD tests were performed using a Rigaku X-ray diffractometer (model: SmartLab) and CuKα (λ = 1.54 Å) radiation was applied. The scanning range of the samples was between 5° and 50°, with a 2θ increase of 0.01° per step.

2.3.3 TGA

TGA was performed to investigate the hydration of the CSA cement-based grouts. The hydration products can be identified by the derivative of weight loss during the heating process [22]. In this study, TGA were conducted on grouts cured at different temperatures for 2 h and 1, 7, and 28 d. The preparation of the samples for the TGA was the same as that for the XRD tests.

TGA was conducted using a Leco TGA 701 instrument. The samples were heated from 20 to 450 °C at a rate of 5 °C/min under a nitrogen atmosphere.

2.3.4 UCS test

In this study, the UCS was determined based on the ASTM-C39 standard [33]. The cylindrical samples (Φ50 mm × 100 mm) were tested using an electro–hydraulic servo pressure testing system, and their UCS at 2 h, 1 d, 3 d, 7 d, and 28 d was obtained.

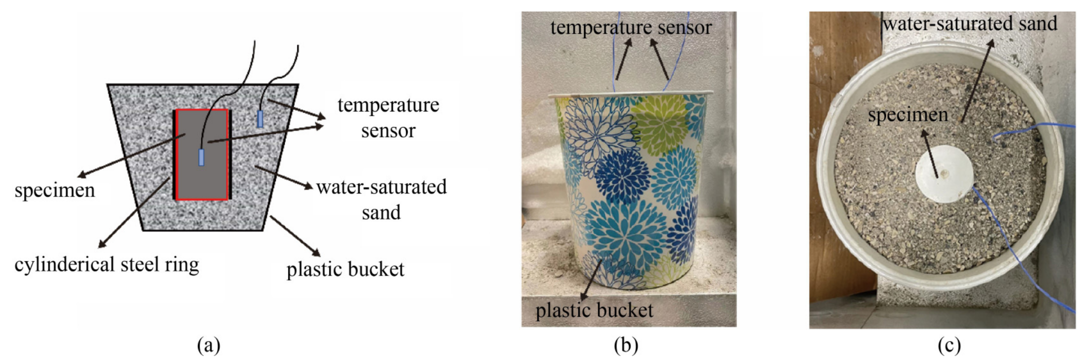

Fig. 1 Curing condition of samples: (a) schematic illustration; (b) side view; (c) plan view.

3 Results and discussion

3.1 Temperature recording analysis

Figure 2 shows the temperature profiles of CSA cement-based grouts under different curing conditions. The temperatures of the samples, sand, and laboratory environment were recorded during the first 48 h. To clearly show the hydration of the samples in the early ages, the temperature profiles of the samples in the first 2 h are presented in zoomed-in figures under each condition.

As shown in Fig. 2(a), the temperature of the sample cured at 20 °C in a laboratory environment increased significantly and peaked within a short time. Initially, the temperature of the sample increased from 19.5 °C to approximately 24.1 °C within 2 min. This process is the initial period, during which cement particles were dissolved and hydrated partially [23,34]. After the initial period, the hydration of the grouts underwent a short induction period and then rapidly reached the acceleration period [35]. During this period, the temperature of the sample increased rapidly and reached 57.5 °C at 36 min, which was almost three times the initial temperature. This shows that the hydration of the CSA cement-based grouts in the early stage was rapid and intensive at the ambient temperature.

The rapid increase in temperature of the samples cured in cold environments occurred at the early stage and not only at the ambient temperature, as depicted in Figs. 2(b)–2(d). The temperature of grouts cured in sand at 10, 0, and −10 °C increased immediately after casting and reached 47.4, 37.8, and 29.8 °C within a short time, respectively. The rapid increase in temperature indicates the rapid hydration of the CSA cement-based grouts at low temperatures. During this process, intensive heat was released to mitigate the undesirable effects of the cold environment on the hydration of the grouts. Meanwhile, the released heat promoted hydration, thus resulting in elevated peak temperatures of the samples. Notably, the temperature of the OPC mortar cured at −10 °C barely increased after the sample was embedded in cold sand [15]. By contrast, a rapid increase in temperature

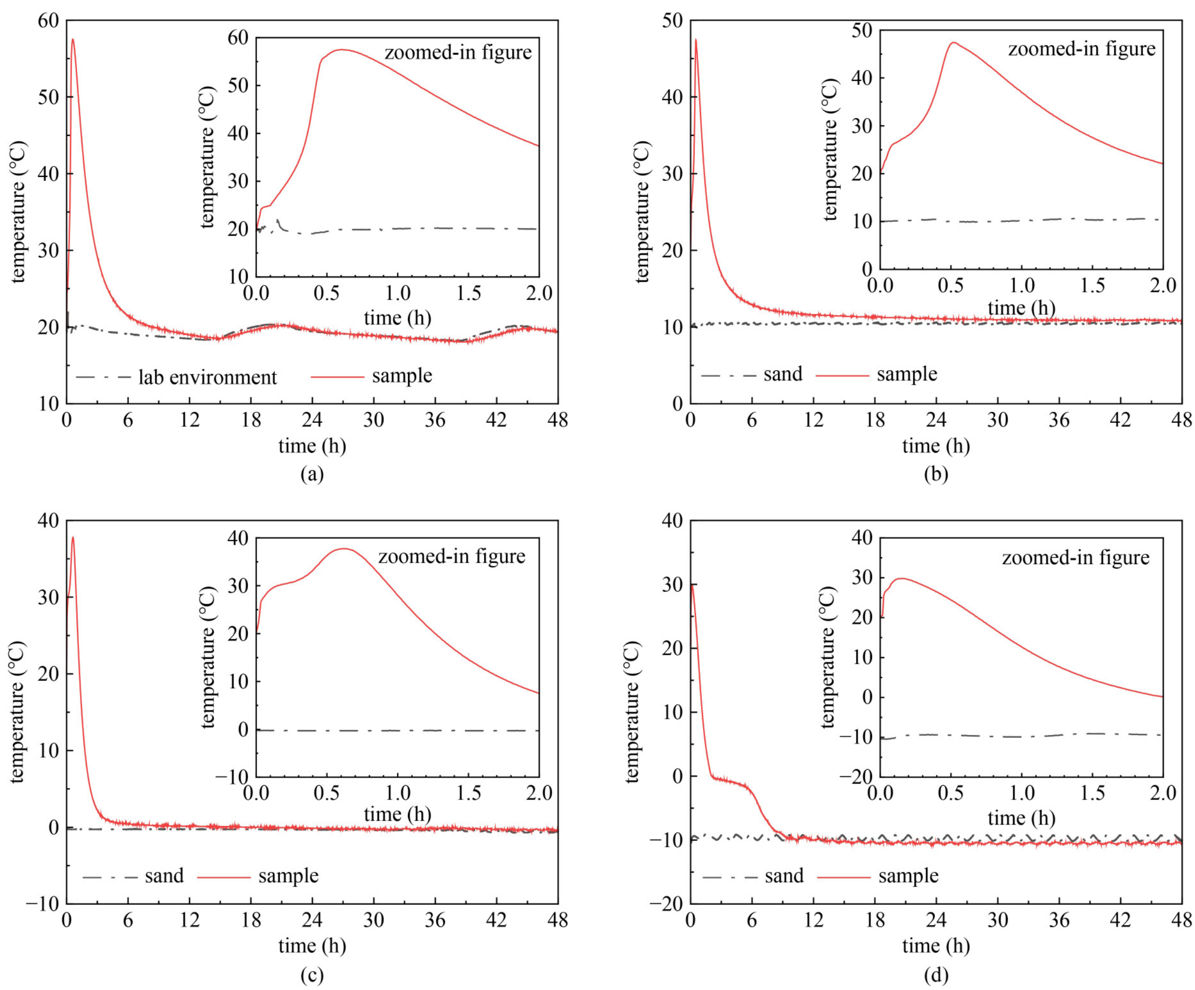

Fig. 2 Temperature records of CSA cement-based grouts cured at (a) 20 °C, (b) 10 °C, (c) 0 °C, and (d) −10 °C.

occurred in the CSA cement-based grouts, even when they were cured at −10 °C, as shown in Fig. 2(d). This implies that CSA cement-based grouts effectively overcome the adverse effects of low temperatures on hydration. Interestingly, a step appeared at 0 °C in the temperature profiles of the sample cured at −10 °C. This step was due to the freezing of water, which released latent heat to mitigate the decrease in temperature [15]. In conclusion, CSA cement-based grouts underwent rapid hydration reactions at the early stage in cold environments.

3.2 XRD test analysis

Figure 3 shows the XRD patterns of CSA cement-based grouts at 2 h and 28 d at various curing temperatures. Ettringite (AFt) was identified as the main hydration product in the CSA cement-based grouts. Other hydration products, such as monosulfate (AFm) and alumina hydroxide (AH_3), were barely detected in the XRD patterns owing to their inferior crystallinity [36]. In addition to the significant quantity of AFt generated, some ye’elimite, belite, and anhydrite were detected in the XRD patterns.

Figure 3(a) shows the effect of curing temperature on each phase of the CSA cement-based grouts after 2 h of curing. The result shows that the type of hydration product remained unchanged although the curing temperature was varied in the early stages. Clear peaks corresponding to AFt were indicated in all the XRD patterns, which implies that the grouts were hydrated at all temperatures within 2 h. However, the amount of hydration products changed considerably with temperature, based on the peak intensity of AFt. The peaks of AFt were the highest in the sample cured at 20 °C, implying that the grouts underwent the highest degree of hydration at that temperature. As the curing temperature decreased, the AFt peaks decreased gradually. As the temperature was reduced to −10 °C, the peaks of AFt descended to its lowest point, which indicates that the hydration rate of the grouts decreased with the curing temperature. Meanwhile, the samples cured at −10 °C exhibited distinct peaks corresponding to AFt. This shows that even though low temperatures hindered hydration, the CSA cement-based grouts remained hydrated at temperatures as low as −10 °C.

Figure 3(b) shows the effect of the curing temperature on each phase of the CSA cement-based grouts at 28 d. Similar to the findings at the early stage, the type of hydration product was not affected by the curing temperature at 28 d. The XRD patterns show that AFt, unhydrated anhydrite, and belite were the dominant crystalline phases in all samples except the sample cured at −10 °C. A slight amount of unhydrated ye’elimite remained in the XRD patterns of the grouts at −10 °C. This shows that, when compared with samples at other curing temperatures, the hydration degree of the grouts was the lowest after they were cured at −10 °C. Compared with the results shown in Fig. 3(a), the quantity of unhydrated products decreased, whereas the quantity of hydration products increased in all groups, including the samples cured at −10 °C. This indicates that the grouts hydrated continuously at low temperatures, even though the hydration rate was low.

3.3 TGA

Figure 4 shows the TGA curves of the CSA cement-based grouts cured at various temperatures at 2 h, 1 d, 7 d, and 28 d. The TGA curves were composed of derivative weight loss and residual weight curves. Depending on the decomposition temperatures, the peaks in the derivative weight loss curves correspond to different types of hydration products. For the CSA cement-based grout samples, two main peaks appeared at approximately 150 and 270 °C, which corresponded to the existence of AFt and AH_3, respectively. Moreover, AFm decomposed at approximately 200 °C. As shown in Fig. 4(a), peaks corresponding to AFt and AH_3 were detected in all the samples at 2 h, even for the grouts cured at low temperatures. This implies that intensive hydration occurred, and a significant quantity of hydration products was formed in the cold environment at the early stage. AFm, which was formed by the hydration of ye’elimite, was detected in all samples. Although the main types of hydration products of CSA cement-based grouts remained constant at all curing temperatures, their quantity was significantly affected by the curing temperature. As shown in Fig. 4(d), the grouts cured at 20 °C indicated the highest peak for AFt at 28 d, whereas the lowest peak was observed for the samples cured at −10 °C, indicating that the generation of AFt decelerated at low temperatures. The peaks for AH_3 were similar for the samples cured at temperatures above 0 °C. This is attributable to the reaction of AH_3 with portlandite (CH) and anhydrite to generate more AFt, based on Eq. (1), and may be the reason that portlandite was not detected in either the XRD or TGA results [30]. In conclusion, although the quantity of hydration products decreased at low temperatures, the CSA cement-based grouts exhibited intensive hydration, particularly at the early stage.

$$AH_3 + 3CH + 3C\bar{S} + 26H \rightarrow C_6A\bar{S}_3H_{32} \quad (1)$$

Owing to the decomposition of the hydration products, the residual weight decreased as the heating temperature increased. When a specific temperature was attained, the residual weight curves showed lower values, indicating that more hydration products were dehydrated during TGA and hence a higher hydration degree of the grouts. Based on Fig. 4(a), the residual weights of the samples at

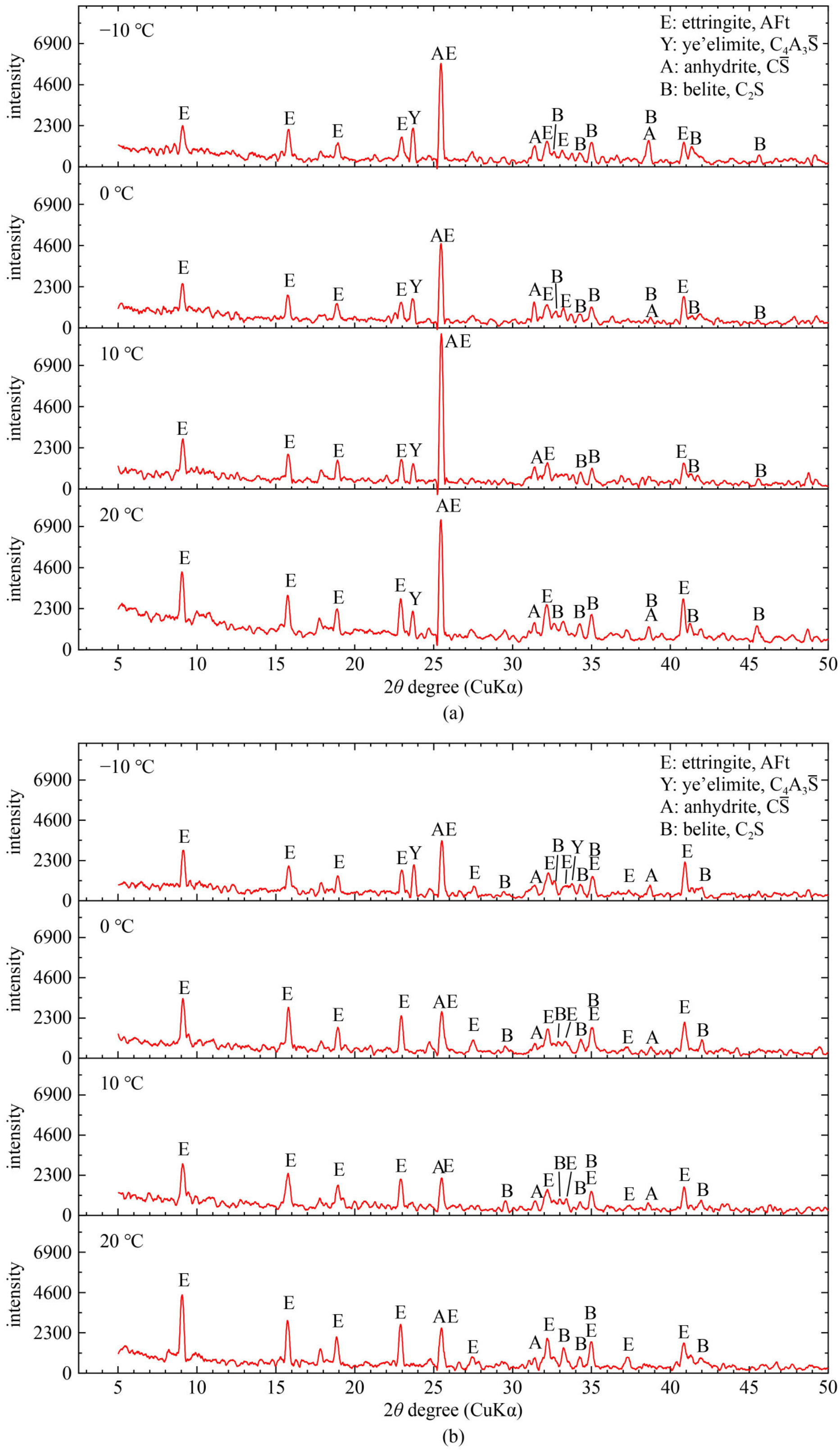

Fig. 3 XRD patterns of CSA cement-based grouts at various curing temperatures: (a) 2 h; (b) 28 d.

different temperatures were similar at 2 h, indicating that the grouts exhibited similar degrees of hydration. This is because the early hydration of the grouts was significantly affected by the placing temperature, which was the same for all samples in this study. Subsequently, a decrease in residual weight was observed in all samples from day 1 to day 28, indicating that the grouts were hydrated continually at all curing temperatures. However,

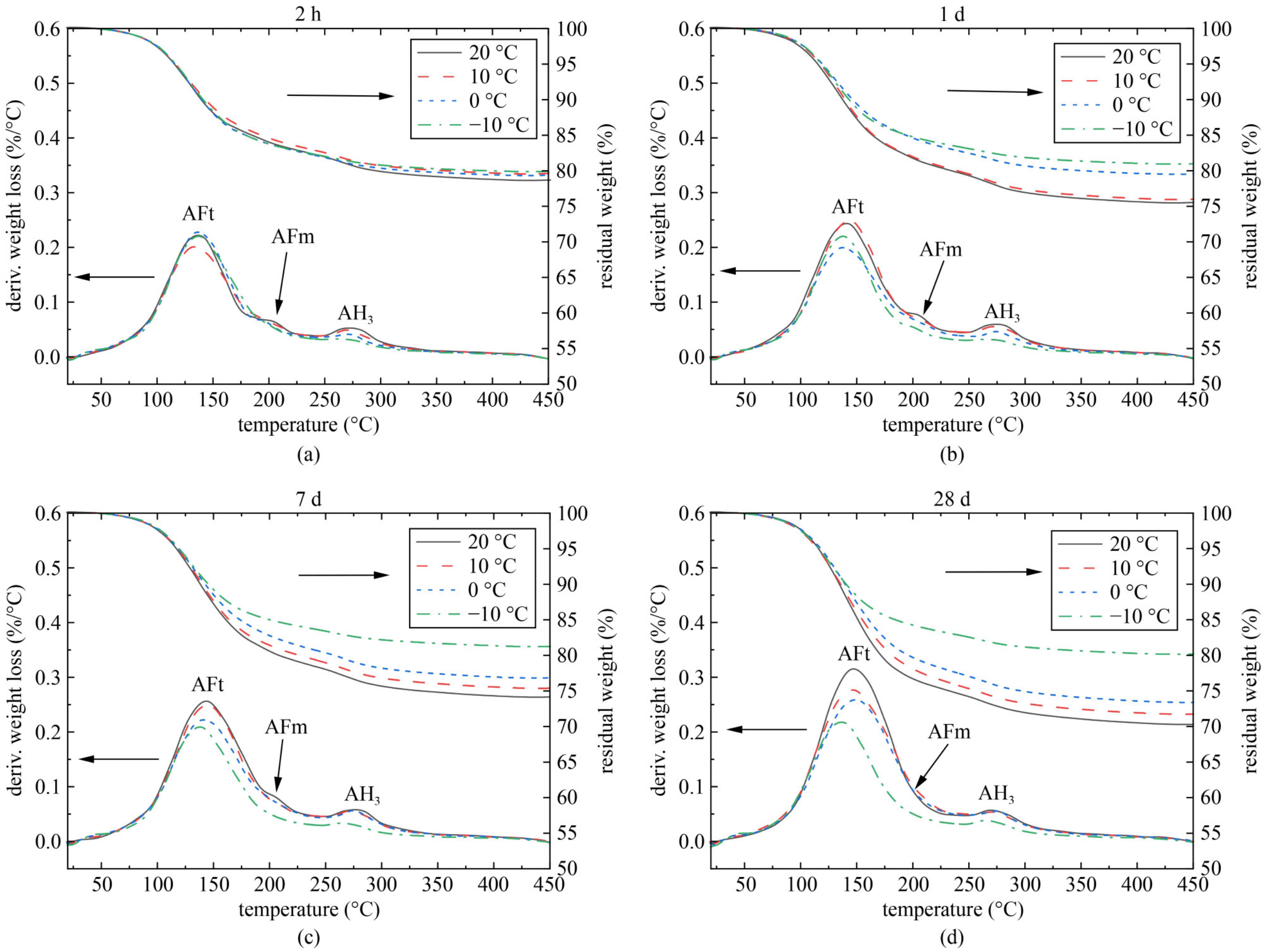

Fig. 4 TGA curves of CSA cement-based grouts at various curing temperatures: (a) 2 h; (b) 1 d; (c) 7 d; (d) 28 d.

the effects of the curing conditions on the hydration degree of the grouts became increasingly significant after 2 h. Based on Figs. 4(b)–4(d), the grouts cured at 20 °C indicated the most significant decrease in residual weight from day 1 to day 28, whereas the least reduction was observed in the sample cured at −10 °C. This implies that temperature significantly affects the hydration degree of the grouts and that a high curing temperature is more conducive to the hydration of the grouts. Notably, most of the weight loss occurred prior to day 1, and the difference in residual weight between days 1 and 28 was less than 5% for the samples cured at all temperatures. This indicates that the CSA cement-based grouts hydrated rapidly and exhibited a considerably high degree of early hydration, including the grouts cured at low temperatures.

3.4 UCS analysis

The effect of the curing temperature on the UCS of CSA cement-based grouts at different curing ages is shown in Fig. 5. The curing temperature exhibited distinct effects on the UCS of the grouts at different ages. At 2 h, the UCS of the samples decreased with the curing temperature. In particular, the UCS of the samples cured for 2 h at 20 °C was 13.8 MPa, which was the highest among all curing temperatures. When the curing temperature was decreased to −10 °C, the UCS of the samples decreased to 6.5 MPa, which was approximately 53% lower than that of the samples cured at 20 °C. These results are consistent with those of previous tests. According to the temperature profiles of the samples, the released hydration heat decreased with the curing temperature during the first 2 h, indicating that hydration was restrained at low temperatures. Consequently, fewer hydration products (e.g., AFt and AH_3) were generated, as shown in the results of the XRD test and TGA, which resulted in a lower UCS. At 28 d, the UCS decreased with the curing temperature, except for the samples cured at 10 °C. This trend can be explained by the results of the XRD test and TGA: the hydration products and hydration degree decreased as the curing temperature decreased. However, the UCS of the samples cured at 10 °C was 8% higher than that cured at 20 °C and was the highest among all samples, which is contrary to the TGA results. This is because the UCS of cementitious materials is affected not only by the quantity of hydration products,

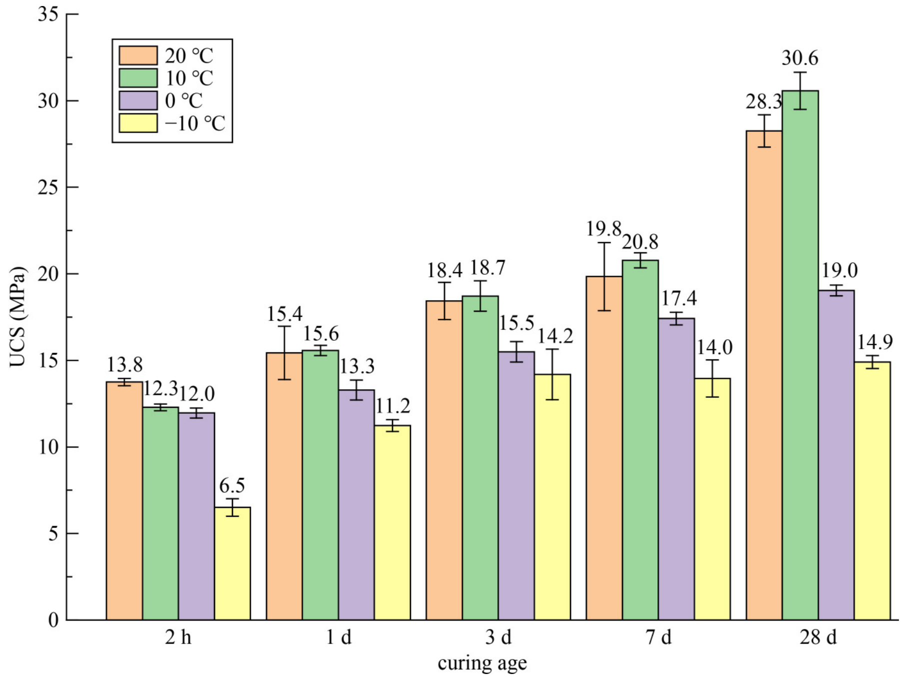

Fig. 5 UCS of CSA cement-based grouts at various curing temperatures.

but also by their shape [4,37,38] and the microstructure of the samples [13,16,39]. When the curing temperature was high, the ettringite crystals appeared slender and needle-shaped, whereas when the curing temperature was decreased, the ettringite crystals transformed to a thicker columnar shape, resulting in a denser microstructure [4,10].

Although low temperatures significantly affect the strength development of grouts, CSA cement-based grouts can still achieve high early-stage strengths in cold environments. Based on Fig. 5, the UCS of the samples cured in sand at 0 °C for 2 h reached 12.0 MPa, which was only 13% lower than that of the samples cured at 20 °C. Moreover, the UCS of the samples cured for 2 h was able to reach 6.5 MPa even when the curing temperature was as low as −10 °C, which demonstrates the rapid strength evolution of the grouts cured in cold environments. By contrast, under similar conditions, mortars prepared with OPC showed almost no strength development after 2 h [15]. The high early UCS of the grouts was due to their fast hydration, from which sufficient hydration products were formed. Based on the recorded temperature and the results of XRD test and TGA, hydration products (e.g., AFt and AH_3) were generated and accumulated at 2 h, accompanied by the release of intensive heat. Because of the rapid strength evolution of the grouts, the 1-d UCS of the samples almost reached 50% of their 28-d UCS at all curing temperatures. The considerably high early strength of the CSA cement-based grouts is advantageous to grouting practices in permafrost environments.

The UCS of the grouts continued to increase with the curing age at all curing temperatures. For the samples cured above 0 °C, the UCS continued to increase with the curing age. The constant strength development of the grouts was attributed to the sustained formation and accumulation of the hydration products. As shown in the XRD and TGA results, the amount of hydration products after 28 d was greater than that at 2 h for each curing temperature. The residual weight based on the TGA decreased as the curing age increased, which suggests an increase in the hydration degree and the continuation of hydration. For the grouts cured below 0 °C, the strength development of the samples was impeded by the cold environment. However, the UCS of the samples reached 14.9 MPa at 28 d when the curing temperature was −10 °C. In conclusion, CSA cement-based grouts demonstrated rapid strength development and excellent strength performance at low temperatures, rendering them promising for permafrost applications.

4 Conclusions

For the first time, the potential of CSA cement-based grouts was appraised in simulated permafrost environments via a combination of tests, including temperature recording, TGA, XRD, and UCS tests. An innovative curing mode, namely, curing samples in cold sand, was adopted to simulate permafrost environments. The performance of the CSA cement-based grouts was evaluated by curing samples in cold sand (10, 0, and −10 °C) and in a laboratory environment (20 °C) as a reference. Based on the results, the key conclusions obtained were as follows.

(1) Rapid temperature increases and extremely high peak temperatures were observed in all samples even at −10 °C, which implies that the hydration of CSA cement-based grouts was rapid and intensive even at freezing temperatures (i.e., 0 and −10 °C).

(2) The types of hydration products of CSA cement-based grouts did not change with the curing temperature.

(3) The CSA cement-based grouts hydrated rapidly and exhibited a high degree of early-age hydration even when the grouts were cured at low temperatures. Hydration continued at low temperatures over time.

(4) The rapid hydration reaction allowed the CSA cement-based grouts to demonstrate high early strength. The UCS values of the grouts cured at −10, 0, 10, and 20 °C were 6.5, 12.0, 12.3, and 13.8 MPa at 2 h, respectively.

(5) Because of continued cement hydration, the UCS of the CSA cement-based grouts increased with the curing age; the UCS values of the grouts cured at −10, 0, 10, and 20 °C were 14.9, 19.0, 30.6, and 28.3 MPa at 28 d, respectively.

(6) The CSA cement-based grouts overcame the slow strength development of grouts used in permafrost environments, thereby increasing the grouting efficiency, ensuring the grouting quality, and improving the safety of workers.

In summary, the CSA cement-based grouts achieved fast hydration and rapid strength development, even when they were cured in simulated permafrost environments, and their strength continued to increase with the curing age. Therefore, CSA cement-based grouts are promising for permafrost applications. In future studies, the effect of additives (e.g., accelerator, retarder, and superplasticizer) on the physical (e.g., workability and setting time) and mechanical properties (e.g., compressive strength, flexural strength, and shear strength) of grouts must be investigated to optimize their performance and satisfy the requirements of different applications.

Acknowledgements This study was supported by a research project (RES0049413) at the University of Alberta. The first author is grateful for the scholarship provided by the China Scholarship Council.

References

1. Zhang Q, Zhang L, Liu R, Li S, Zhang Q. Grouting mechanism of quick setting slurry in rock fissure with consideration of viscosity variation with space. Tunnelling and Underground Space Technology, 2017, 70: 262−273
2. Dayakar P, Raman K V, Raju K. Study on permeation grouting using cement grout in sandy soil. IOSR Journal of Mechanical and Civil Engineering, 2012, 4(4): 5−10
3. Li S, Liu R, Zhang Q, Zhang X. Protection against water or mud inrush in tunnels by grouting: A review. Journal of Rock Mechanics and Geotechnical Engineering, 2016, 8(5): 753−766
4. Zhang Y, Li T, Feng W, Xiong Z, Zhang G. Effects of temperature on performances and hydration process of sulphoaluminate cement-based dual liquid grouting material and its mechanisms. Journal of Thermal Analysis and Calorimetry, 2020, 139(1): 47−56
5. Zuo J, Hong Z, Xiong Z, Wang C, Song H. Influence of different *W*/*C* on the performances and hydration progress of dual liquid high water backfilling material. Construction & Building Materials, 2018, 190: 910−917
6. Wang C, Li X, Xiong Z, Wang C, Su C, Zhang Y. Experimental study on the effect of grouting reinforcement on the shear strength of a fractured rock mass. PLoS One, 2019, 14(8): e0220643
7. Nguyen V H, Remond S, Gallias J L. Influence of cement grouts composition on the rheological behaviour. Cement and Concrete Research, 2011, 41(3): 292−300
8. Azadi M R, Taghichian A, Taheri A. Optimization of cement-based grouts using chemical additives. Journal of Rock Mechanics and Geotechnical Engineering, 2017, 9(4): 623−637
9. Bohloli B, Skjølsvold O, Justnes H, Olsson R, Grøv E, Aarset A. Cements for tunnel grouting—Rheology and flow properties tested at different temperatures. Tunnelling and Underground Space Technology, 2019, 91: 103011
10. Borštnar M, Daneu N, Dolenec S. Phase development and hydration kinetics of belite-calcium sulfoaluminate cements at different curing temperatures. Ceramics International, 2020, 46(18): 29421−29428
11. Dobinski W. Permafrost. Earth-Science Reviews, 2011, 108(3–4): 158–169
12. Biggar K W, Sego D C, Noël M M. Laboratory and field performance of high alumina cement-based grout for piling in permafrost. Canadian Journal of Civil Engineering, 1993, 20(1): 100−106
13. Xu W, Zhang Y, Liu B. Influence of silica fume and low curing temperature on mechanical property of cemented paste backfill. Construction & Building Materials, 2020, 254: 1−10
14. Jakubec J, Lagace D, Boggis B, Clark L M, Lewis P A. Underground mining at Ekati and Diavik diamond mines. In: Caving 2018: Proceedings of the Fourth International Symposium on Block and Sublevel Caving. Perth: Australian Centre for Geomechanics, 2018, 73−88
15. Huang G, Pudasainee D, Gupta R, Liu W V. Hydration reaction and strength development of calcium sulfoaluminate cement-based mortar cured at cold temperatures. Construction & Building Materials, 2019, 224: 493−503
16. Zhang G, Yang Y, Yang H, Li H. Calcium sulphoaluminate cement used as mineral accelerator to improve the property of Portland cement at sub-zero temperature. Cement and Concrete Composites, 2020, 106: 103452
17. Xu L, Wu K, Rößler C, Wang P, Ludwig H M. Influence of curing temperatures on the hydration of calcium aluminate cement/Portland cement/calcium sulfate blends. Cement and Concrete Composites, 2017, 80: 298−306
18. Huang G, Pudasainee D, Gupta R, Liu W V. Extending blending proportions of ordinary Portland cement and calcium sulfoaluminate cement blends: Its effects on setting, workability, and strength development. Frontiers of Structural and Civil Engineering, 2021, 15(5): 1249−1260

19. Winnefeld F, Lothenbach B. Hydration of calcium sulfoaluminate cements—Experimental findings and thermodynamic modelling. Cement and Concrete Research, 2010, 40(8): 1239−1247
20. Berger S, Coumes C C D, Le Bescop P, Damidot D. Influence of a thermal cycle at early age on the hydration of calcium sulphoaluminate cements with variable gypsum contents. Cement and Concrete Research, 2011, 41(2): 149−160
21. Martín-Sedeño M C, Cuberos A J M, De la Torre Á G, Álvarez-Pinazo G, Ordónez L M, Gateshki M, Aranda M A G. Aluminum-rich belite sulfoaluminate cements: Clinkering and early age hydration. Cement and Concrete Research, 2010, 40(3): 359−369
22. Winnefeld F, Martin L H J, Müller C J, Lothenbach B. Using gypsum to control hydration kinetics of CSA cements. Construction & Building Materials, 2017, 155: 154−163
23. Tang S W, Zhu H G, Li Z J, Chen E, Shao H Y. Hydration stage identification and phase transformation of calcium sulfoaluminate cement at early age. Construction & Building Materials, 2015, 75: 11−18
24. Zhang J, Guan X, Wang X, Ma X, Li Z, Xu Z, Jin B. Microstructure and properties of sulfoaluminate cement-based grouting materials: Effect of calcium sulfate variety. Advances in Materials Science and Engineering, 2020, 2020: 1−8
25. Kaufmann J, Winnefeld F, Lothenbach B. Stability of ettringite in CSA cement at elevated temperatures. Advances in Cement Research, 2016, 28(4): 251−261
26. Zhang Y, Chang J, Ji J. AH_3 phase in the hydration product system of AFt-AFm-AH_3 in calcium sulfoaluminate cements: A microstructural study. Construction & Building Materials, 2018, 167: 587−596
27. Zhang J, Guan X, Li H, Liu X. Performance and hydration study of ultra-fine sulfoaluminate cement-based double liquid grouting material. Construction & Building Materials, 2017, 132: 262−270
28. Zhang Y, Wang Y, Li T, Xiong Z, Sun Y. Effects of lithium carbonate on performances of sulphoaluminate cement-based dual liquid high water material and its mechanisms. Construction & Building Materials, 2018, 161: 374−380
29. Li H, Yang K, Guan X. Properties of sulfoaluminate cement-based grouting materials modified with LiAl-layered double hydroxides in the presence of PCE superplasticizer. Construction & Building Materials, 2019, 226: 399−405
30. Wang Y, Yu J, Wang J, Guan X. Effects of aluminum sulfate and quicklime/fluorgypsum ratio on the properties of calcium sulfoaluminate (CSA) cement-based double liquid grouting materials. Materials (Basel), 2019, 12(8): 1222
31. Slusarchuk W A, Watson G H. Thermal conductivity of some ice rich permafrost soils. Canadian Geotechnical Journal, 1975, 12(3): 413−424
32. Romanovsky V, Osterkamp T. Thawing of the active layer on the coastal plain of the Alaskan Arctic. Permafrost and Periglacial Processes, 1997, 8(1): 1−22
33. ASTM C39/C39M-21. Standard test method for compressive strength of cylindrical concrete specimens. West Conshohocken: ASTM International, 2021
34. Zhang L, Glasser F. Hydration of calcium sulfoaluminate cement at less than 24 h. Advances in Cement Research, 2002, 14(4): 141−155
35. Bullard J W, Jennings H M, Livingston R A, Nonat A, Scherer G W, Schweitzer J S, Scrivener K L, Thomas J J. Mechanisms of cement hydration. Cement and Concrete Research, 2011, 41(12): 1208−1223
36. Song F, Yu Z, Yang F, Lu Y, Liu Y. Microstructure of amorphous aluminum hydroxide in belite-calcium sulfoaluminate cement. Cement and Concrete Research, 2015, 71: 1−6
37. Guo W, Qiu J, Chen Q, Wang X, Yang T. Low-temperature calcination of belite-calcium sulphoaluminate cement clinker and the hydration process. Journal of Materials in Civil Engineering, 2021, 33(12): 04021350
38. Li P, Gao X, Wang K, Tam V W Y, Li W. Hydration mechanism and early frost resistance of calcium sulfoaluminate cement concrete. Construction & Building Materials, 2020, 239: 117862
39. Wang P, Li N, Xu L. Hydration evolution and compressive strength of calcium sulphoaluminate cement constantly cured over the temperature range of 0 to 80 °C. Cement and Concrete Research, 2017, 100: 203−213